Mechanically Tunable Hollow Silica Ultrathin Nanoshells for Ultrasound Contrast Agents

*A. Liberman, James Wang, N. Lu, Robert D. Viveros, C. A. Allen, R. F. Mattrey, S. L. Blair, W. C. Trogler, M. J. Kim, and A. C. Kummel**

Perfluoropentane (PFP) gas-filled biodegradable iron-doped silica nanoshells have been demonstrated as long-lived ultrasound contrast agents. Nanoshells are synthesized by a sol–gel process with tetramethyl orthosilicate (TMOS) and iron ethoxide. Substituting a fraction of the TMOS with R-substituted-trialkoxysilanes produces ultrathin nanoshells with varying shell thicknesses and morphologies composed of fused nanoflakes. The ultrathin nanoshells have continuous ultrasound Doppler imaging lifetimes exceeding 3 h, are twice as bright using contrast-specific imaging, and have decreased pressure thresholds compared to control nanoshells synthesized with just TMOS. Transmission electron microscopy shows that the R-group-substituted trialkoxysilanes can reduce the mechanically critical nanoshell layer to 1.4 nm. These ultrathin nanoshells have the mechanical behavior of weakly linked nanoflakes but the chemical stability of silica. The synthesis can be adapted for general fabrication of 3D nanostructures composed of nanoflakes, which have thicknesses from 1.4 to 3.8 nm and diameters from 2 to 23 nm.

1. Introduction

Silica has been an attractive material used in nanomedicine research for applications, such as drug delivery,[1,2] protein/enzyme delivery,[3] and biomedical imaging.[4] Studies of medical applications of silica nanoparticles have been aided by the numerous synthetic techniques available to form particles with diverse sizes and structures[5,6] and robust in vivo stability and minimal toxicity.[7,8] Different materials, such as surfactants and organically modified silanes, have been incorporated into the synthesis of silica nanoparticles to control their structures or sizes. For example, surfactants such as cetyltrimethylammonium bromide (CTAB) or various polymers are used in order to generate mesoporous silica nanoparticles.[9] In addition to tetraalkoxysilanes, various mono-, bi-, and tri- substituted alkoxysilanes have been co-condensed to form silica nanoparticles. Typically these substituted alkoxysilanes are used to functionalize silica nanoparticles;[2,8,10] however, they have also been used in particle synthesis.[11]

Other sol–gel compatible materials have also been co-condensed with tetraalkoxysilane. For example, Mitchell et al.[12] added iron (III) ethoxide during the synthesis of silica nanoshells to generate shells that break down in the presence of iron (III) chelating proteins. Martinez et al.[13] co-condensed trimethyl borate with tetramethyl orthosilicate (TMOS) to prepare microshells, which were mechanically strengthened by incorporating boron into the silica network. Several reports have specifically investigated the mechanical properties of nanoparticle formulations. Zhang et al.[14] had previously synthesized silica nanoshells, which were tested by atomic force microscopy (AFM); it was found that particles with shell thickness as thin as 15 nm had the same Young's modulus as bulk silica. It was also observed that the minimum force necessary to cause deformation in the silica shells increased as a function of the shell thickness squared.

Silica nanoparticle growth can be modeled using a LaMer model[15] in which at a critical free energy, nanoparticles of a critical radius begin to form, which depends on concentration

A. Liberman
Materials Sciences and Engineering Program
University of California
San Diego, CA 92093, USA
J. Wang, R. D. Viveros
Department of Nanoengineering
University of California
San Diego, CA 92093, USA
Dr. N. Lu, Prof. M. J. Kim
Department of Materials Science and Engineering
The University of Texas at Dallas
Richardson, TX 75080, USA

DOI: 10.1002/adfm.201500610

C. A. Allen, Prof. W. C. Trogler, Prof. A. C. Kummel
Department of Chemistry and Biochemistry
University of California
San Diego, CA 92093, USA
E-mail: akummel@ucsd.edu
Prof. R. F. Mattrey
Department of Radiology
University of California
San Diego, CA 92093, USA
Prof. S. L. Blair
Moores Cancer Center
University of California
San Diego, CA 92093, USA

of precursor and other parameters. For silica, nanoparticles may result from either continued growth of nuclei or by agglomeration of smaller nuclei. Caruso et al.[6] demonstrated that silica nanoshells could be synthesized by adsorbing 25 nm silica nanoparticles onto positively charged polystyrene templates and calcining them to produce hollow silica nanoshells. This demonstrates that silica nanoparticles can be constructed in a hierarchical fashion similar to various nanoflake–nanoparticle formulations. The term nanoflake has been used to describe nanomaterials that are 2D with diameters or cross sections ranging from 1 to 500 nm. Nanoflake thicknesses typically fall in the sub-20 nm range with Mazur[16] reporting on silver nanoflakes as thin as 0.5 nm. Nanoflakes have been synthesized from a wide variety of materials for a spectrum of applications, such as improving electronic properties of materials or modifying thermal properties.[17] For example, Cui et al.[18] showed that 100–200 nm diameter ceria (CeO_2) nanoparticles synthesized for catalysis were actually composed of an aggregate of 10 × 20 nm nanoflakes. These results suggest that it may be possible to synthesize silica nanoparticles composed of a hierarchical structure of nanoflakes.

There are many applications of silica nanostructures, including ultrasound contrast agents. These agents are typically synthesized by encapsulating a perfluorocarbon gas within a lipid or polymeric shell to produce elastic microbubbles in the range 1–6 µm in diameter.[19] When insonated, these microbubbles oscillate to produce signals at harmonic frequencies and, at resonance, break into smaller bubbles and collapse producing a broadband signal.[20] Since tissues only reflect the primary insonating frequency, contrast-specific imaging provides a microbubble only image, which displays the location of the contrast agent on the image. Recently, there have been several examples of silica-based nanoparticle formulations that can also be used for contrast-enhanced ultrasound. It was previously demonstrated that perfluoropentane (PFP) gas entirely fills the particles and that the volume of gas within the particles has an effect on the quality of the ultrasound signal.[13] The volume fraction of particle occupied by the shell only accounts for a small fraction of the total volume of each particle. Hollow silica gas-filled particles have a large acoustic impedance mismatch between the surrounding fluid/tissue environment, which makes them readily observable under ultrasound.[21] The nanoshell's primary function is as a carrier for the gas; the expansion, release, and potential oscillation of this gas are what results in the contrast ultrasound signal. The greatest advantage in using silica nanoparticles as ultrasound contrast agents compared to traditional liposomal/polymeric imaging agents is their improved in vivo stabilities and long imaging lifetimes. For example, gas-filled silica particles could be continuously imaged for 45 min.[22] Iron–silica nanoshells filled with PFP could be imaged intermittently over the course of 10 d in a tumor-bearing mouse with color Doppler imaging after intratumoral delivery of nanoshells.[23]

Ultrasound imaging power is referred to as mechanical index (MI), which is proportional to the peak negative pressure divided by the square root of the imaging frequency. Since silica particles produced greater signal as the MI was increased, it was proposed that there must be subpopulations of particles with varying mechanical strengths that fracture to release the gas at different pressures.[22] The shell provides a layer of shielding between the gas and the incoming ultrasound pulse. As a result, it is necessary to synthesize nanoshells with a larger percentage of the subpopulations that are mechanically weaker so that the ensemble can be imaged at lower MI for longer times. This was achieved by modifying the nanoshell synthesis with organically modified trialkoxysilanes which produced nanoshells composed of an assembly of ultrathin nanoflakes. The ultrathin nanoshells had significantly lower color Doppler imaging thresholds, greater imaging longevities, and greater contrast-specific imaging performance derived from improved nanostructures compared to control nanoshells made with only TMOS and thus thicker shells.

2. Results and Discussion

The structures of the organically modified trialkoxysilanes used in synthesis of the nanoshells can be viewed in **Figure 1**. Scanning electron microscopy (SEM) images show (**Figure 2**) that all formulations produce uniform 500 nm nanoshells; however, there are key structural differences between the advanced formulations compared with the **control** iron-doped silica nanoshells, which use 100% TMOS as the silica precursor (Figure 2A). a) The surface morphology of the triethoxy(octyl)silane (**C8**) (Figure 2B) and trimethoxyphenylsilane (**phenyl**) (Figure 2D) particles is smoother than the other formulations. b) For only the **C8** and **phenyl** formulations, the first layer of nanoshells is sufficiently transparent in SEM to observe the underlying second layer of particles, which is consistent with thinner shell walls. The **control** nanoshells, 1H,1H,2H,2H-perfluorooctyltriethoxysilane

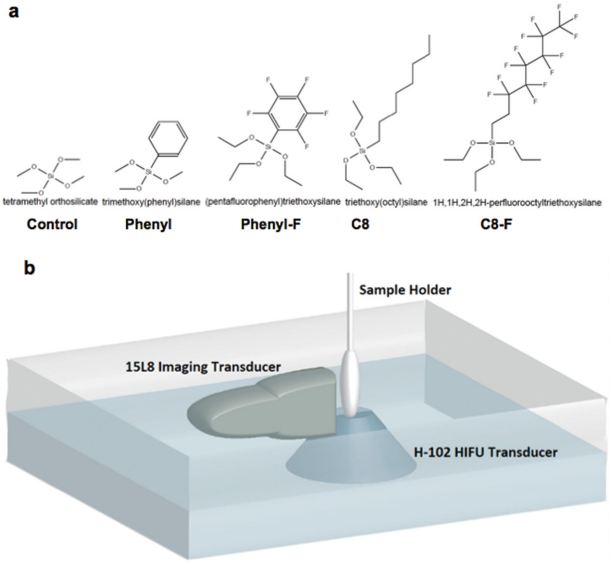

Figure 1. Structures of R-group-substituted trialkoxysilanes and experimental setup for ultrasound testing of nanoshells. A) Molecular structures and naming scheme of R-group-substituted trialkoxysilanes used in the modified sol–gel synthesis. B) Experimental setup for ultrasound testing of nanoshells. Nanoshells were suspended in the sample holder at 400 µg mL^{-1}. The imaging transducer and the HIFU transducer were aligned orthogonally.

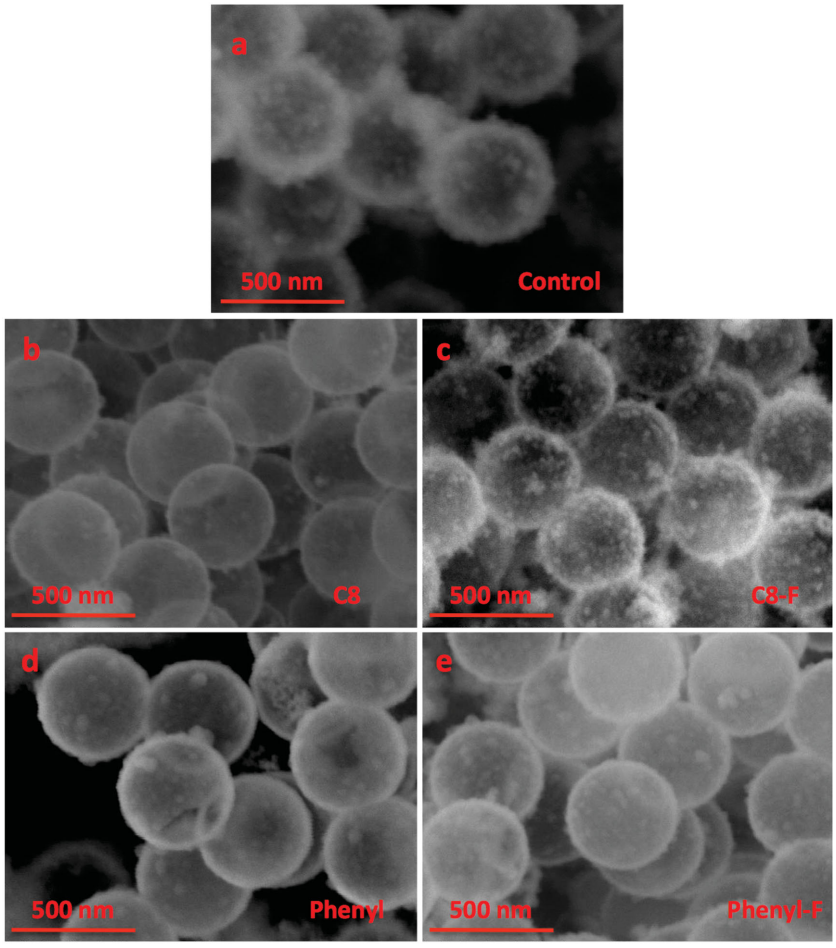

Figure 2. Scanning electron microscopy of various formulations at 74 K magnification after nanoshells have been calcined. A) Control nanoshells. B) Nanoshells synthesized with C8. C) Nanoshells synthesized with C8-F. D) Nanoshells synthesized with phenyl. E) Nanoshells synthesized with phenyl-F. The transparent images of the C8 and phenyl particles are consistent with the nanoflakes-forming shells of a few nanometer thickness.

(**C8-F**) nanoshells, and (pentafluorophenyl)triethoxysilane (**phenyl-F**) nanoshells have a layer of flaked silica on the outer surface of the nanoshell.

Iron–silica nanoshells were developed as an intraoperative color Doppler tumor marker, and nanoshells were characterized at 7 MHz, the previously determined optimal frequency, for color Doppler imaging threshold and continuous imaging longevity in vitro.[13,22,23] As shown in **Figure 3**A, the **phenyl**, **C8**, and **C8-F** formulations had a lower MI threshold compared to the control particles. This is consistent with the particles being more sensitive to color Doppler imaging and consistent with the thinner shells observed for these formulations in SEM. The mechanism for color Doppler imaging of the rigid nanoshells has been shown to arise from nanoparticle fracture and release of entrapped perfluorocarbon gas.[13,22] To measure the continuous imaging lifetime (Figure 3B), particles were imaged continuously at MI 1.9 until no signal could be generated from the sample. For the **phenyl** and the **C8** particles, signal continued to be readily observed at 180 min (Figure 3C,D). Since the same mass of particle was tested for all formulations, the differences in intensities and imaging lifetimes suggest that they arise from the differences in subpopulations of particles being imaged. It is hypothesized that for the **control**, **phenyl-F**, and **C8-F** particles, large fractions of particles are too mechanically robust to be shattered during insonation and as such do not generate any ultrasound contrast signal. It is hypothesized that a greater fraction of **phenyl** and the **C8** particles are weakened as a result of thinner shells and thus have more ultrasound-active particles per unit mass. A larger number of ultrasound-sensitive particles result in a much longer imaging lifetime.

To quantitatively test the hypothesis that a different subpopulation of particles was being imaged at each MI, image brightness on contrast-specific imaging was plotted over time

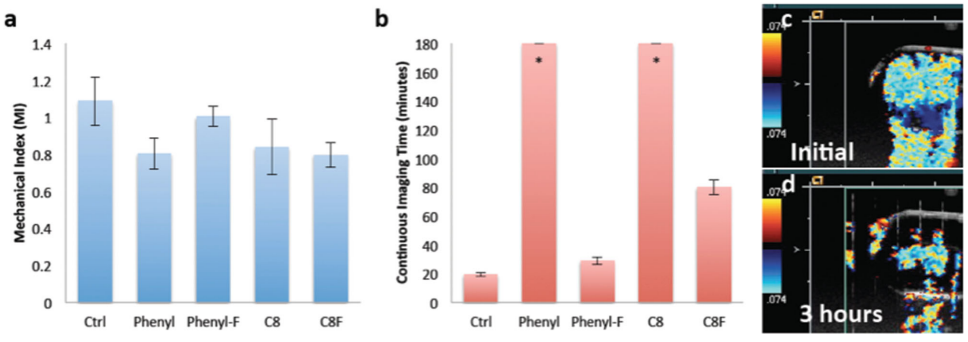

Figure 3. Color Doppler ultrasound testing of nanoshells. A) Mean MI threshold to generate color Doppler signal, the error bars signify standard deviation. B) Imaging lifetime in minutes of nanoshell formulations with continuous color Doppler imaging at MI = 1.9, error bars signify standard deviations. *Note that the **phenyl** and **C8** particles had no standard deviations because the test was terminated at 180 min. C) Color Doppler signal from **C8** nanoshells detected at the initiation of the continuous imaging study. D) Color Doppler imaging of the same **C8** suspension at 180 min. Note that although the signal decreases after 180 min, it was still robust. The long imaging times of the **C8** and **phenyl** particles correlate with these having the thinnest shell walls as shown in SEM and TEM imaging.

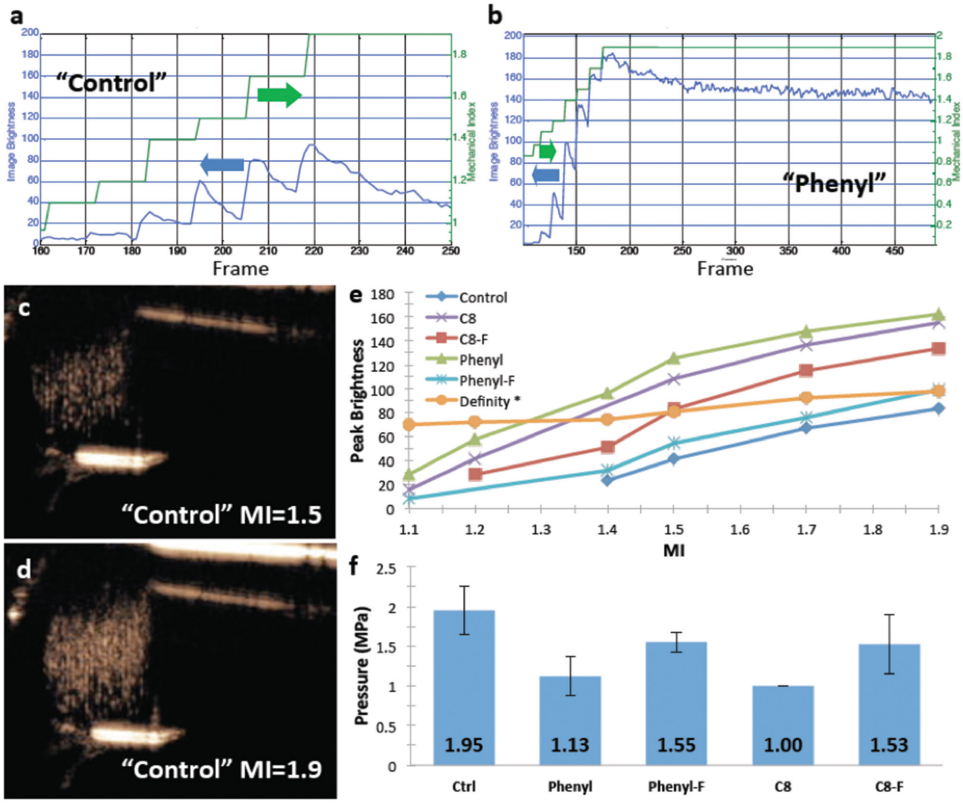

Figure 4. Image brightness over time with CPS imaging as a function of MI of PFP gas-filled nanoshells. A) Signal brightness plotted with mechanical index as a function of time (frames) for **control** nanoshells. B) Signal brightness and mechanical index as a function of time (frames) for **phenyl** nanoshells. Note that with each MI step, brightness increases and then decays until the next MI step. Also note the greater signal generated with the **phenyl** formulation at each MI and the slower decay even at maximum MI of 1.9. C) CPS image of **control** nanoshells acquired at MI = 1.5. D) CPS image of **control** nanoshells acquired at MI = 1.9. Note the greater brightness at 1.9 MI. E) is a plot of peak brightness on CPS images as a function of MI for all formulations. Note that the Phenyl formulation had a relatively low threshold and generated the brightest signal at all MIs. *Note: The sample gas volumes occupied between the nanoshells and Definity are equal; however, the Definity particle count is 64 times less than the nanoshells due to their larger size. F) Pressure threshold of the HIFU pulse that generated signal on the CPS image. Error bars signify standard deviations, $N = 5$. Individual plots with standard deviations can be seen in Figure S1 (Supporting Information). It should be noted that the brightness is log compressed.

(or frame number) for all the formulations; note this is a log scale. **Figure 4**A,B shows signal brightness (blue curve) at each MI (green stepwise line) for the **control** and **phenyl** nanoshells. Note that signal increases as the MI is increased followed by signal decay as particles of a given sensitivity are consumed. Figure 4C,D is representative contrast pulse sequencing (CPS) ultrasound images of the **control** nanoshells at two different MI settings. Increasing the MI increases image brightness, which is seen as gold speckles on CPS imaging. As shown in Figure 4A,B, for an equivalent mass of particles, the **phenyl** particles are approximately twice as bright (on a log scale) at peak brightness compared to the **control** particles. Furthermore, the signal in CPS mode does not experience as much signal decay for the **phenyl** nanoshells and persists at a brightness of 160 for several minutes compared to an immediate decay to below 40 for the **control** particles. The difference in imaging persistence between CPS imaging and color Doppler imaging is consistent with the CPS waveform being less destructive than the color Doppler waveform.

Figure 4E shows peak brightness as a function of MI for each formulation; **phenyl**, **C8**, and **phenyl-F** formulations produced signal at lower thresholds compared to other formulations, and the **phenyl** and **C8** formulations produced the brightest signals. Note that ultrasound signals are log compressed to display the entire dynamic range on the video monitor. Therefore, the observed differences in brightness, as shown in Figure 4, are quite large.[24] Previous reports suggested that the peak-decay behavior of the control nanoshells at varying MI (as shown in Figure 4A) is consistent with the control particles having different subpopulations with varying mechanical strengths. The present data are consistent with different R-substituted trialkoxysilanes decreasing the average mechanical strength of the nanoshells, thereby allowing a brighter signal as well as an increased imaging longevity. For comparison, commercially available Definity microbubbles were diluted to an approximately equivalent gas volume as occupied by the nanoshells and compared directly to the nanoshells. This was done by particle volume because on average individual Definity microbubbles have a diameter between 1 and 3 µm, which results in a 64 times greater volume per particle than the nanoshells. It should be noted that in this MI regime, Definity microbubbles are being destroyed similar to the nanoshells. However, unlike the nanoshell samples where the MI was slowly raised from 0.06 to 1.9 for each sample, each

measurement on Definity microbubbles at each MI was done using a pristine sample due to the short imaging lifetime of Definity. An MI of 1.9 is the maximum power used on clinical ultrasound imaging systems. It is evident from this data that the **C8** and the **phenyl** nanoshells generate more contrast at MIs greater than 1.3 than Definity. To the authors' knowledge this is the first report of any rigid particle demonstrating a signal comparable to a commercially available contrast agent in a contrast-specific imaging modality. This illustrates the unique properties that can be generated from nanostructures made of the ultrathin nanoflakes.

To determine the factors that influence the ultrasound signal threshold and intensity, 20 μs pulses at 1.1 MHz were delivered to the sample by the high-intensity focused ultrasound (HIFU) transducer to fracture and release the PFP gas as the sample was simultaneously being imaged in CPS mode at 0.1 MI to detect the freed PFP bubbles using the apparatus shown in Figure 1. Note that the 0.1 MI power is well below the signal generation threshold for all the formulations (Figure 4E). As shown in Figure 4F, all the formulations synthesized with the R-substituted trialkoxysilanes had a lower pressure threshold compared to the **control** nanoshells. The **C8** nanoshells had the lowest pressure threshold, but this was not statistically different from the threshold of the **phenyl** nanoshells, both of which had a threshold ≈50% that of the **control**. This demonstrates that use of ultrathin nanoflakes can be used for modifying the mechanical properties of 3D structures.

An in vivo experiment was performed in VX2 tumor-bearing rabbits using a slightly modified ultrathin **phenyl** nanoshell formulation with a 55:45 molar ratio of trimethoxy(phenyl) silane:TMOS ratio. This ratio was used due to improved synthetic yield. 100 μL of nanoshells at 4 mg mL^{-1} was injected intratumorally and imaged over the course of 13 d. As can be seen from **Figure 5**, the signal remains easily detectable through at least 11 d by color Doppler imaging. Previous work by our group describes the **control** particles as having lasted for 10 d in PY8119 epithelial breast tumor bearing mice, and pure silica particles are imageable in rabbit thighs after intramuscular injection for only 4 d.[22,23] Unlike the mouse tumors, which are very poorly vascularized and isolated from motion, the VX2 model is well vascularized; furthermore, these tumors were subject to extensive motion because the tumors were grown in the thigh muscles. Vascularization provides a means for both the particles and the encapsulated gas to escape. As a result, this is a realistic test of in vivo lifetime for intratumoral injection.

To further investigate the source of the mechanism of improved ultrasound performance, transmission electron microscopy (TEM) imaging was performed. The images in **Figure 6** are consistent with all formulations of nanoshells being composed of fused silica nanoflakes, which are linked together by condensation of surface silanol groups after they assemble on the template surface. These nanoflakes are formed initially during the sol–gel process and are present before calcination (see TEM image of control particles nanoflakes in Figure S2, Supporting Information). As can be seen from the TEM images, there is no clear pore structure throughout the nanoshells. It is likely that the PFP gas that fills the particles enters through the grain boundaries between weakly

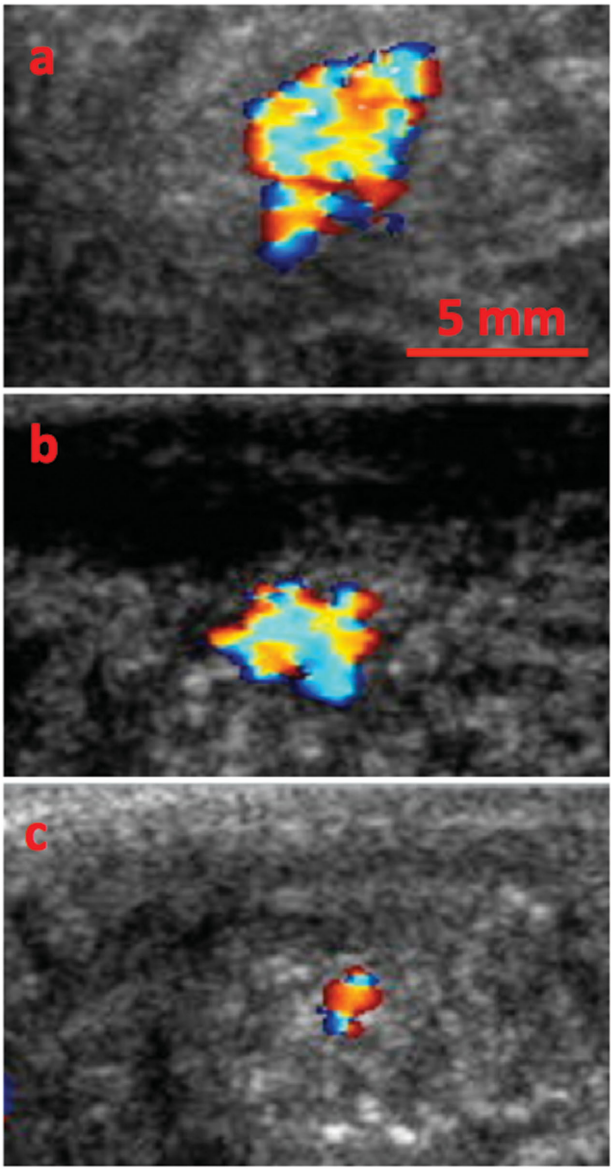

Figure 5. Intratumoral nanoshell longevity. 100 μL of nanoshells at 4 mg mL^{-1} was injected intratumorally into VX2 tumor-bearing rabbits and imaged over the course of 13 d. A) 1 d after injection. B) 6 d after injection. C) 11 d after injection.

linked nanoflakes or through subnanometer pores that cannot be resolved by TEM. As shown in Figure 6, the formulations synthesized with R-substituted trialkoxysilanes had markedly thinner shells than the **control** formulation and, therefore, are denoted as ultrathin nanoshells. The thinner walls of the ultrathin nanoshells result mechanically weaker shells than the thick-walled **control** nanoshells.

One potential source of the variation in structure and properties observed could be from varying degrees of reactivities or varying degrees of polycondensation among the different alkoxysilanes. These properties would result in different molar ratios of the organosilane incorporating to the silica shell compared to the starting amounts added. This could result in particles of different shell thicknesses, mechanical properties, and

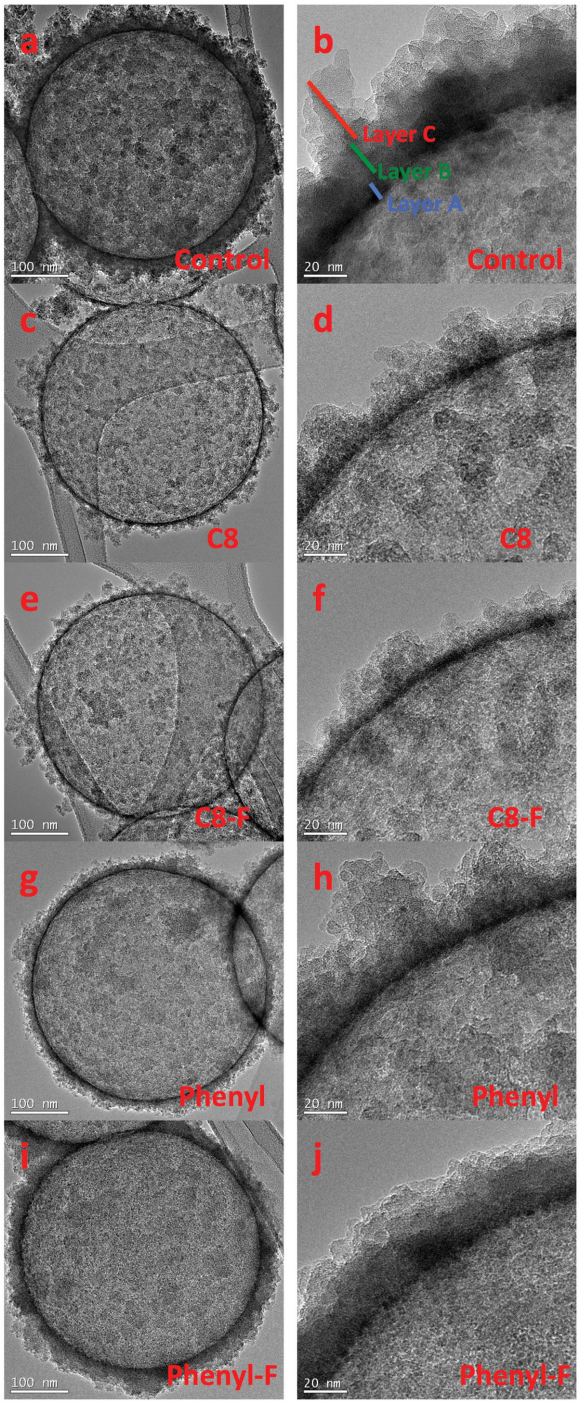

Figure 6. TEM images of all nanoshell formulations. All images were taken at 40 000× magnification and then 150 000× magnification for high-resolution images of the shells. A,B) **Control** nanoshells. C,D) Nanoshells synthesized with **C8**. E,F) Nanoshells synthesized with **C8-F**. G,H) Nanoshells synthesized with **phenyl**. I,J) Nanoshells synthesized with **phenyl-F**. The nanoshells synthesized with **C8 and phenyl** had the thinnest walls.

differing sized nanoflakes. It is known that long-chain alkyl and aromatic side groups of trialkoxysilanes will reduce the rate of hydrolysis and polycondensation due to their electron-donating characteristic.[25] For example, it has been shown that under neutral conditions without a catalyst (acid, base, metal alkoxides, etc.), triethoxy(octyl)silane undergoes very little hydrolysis, which is necessary for polycondensation to occur.[26] Alternatively, the high electronegativity from the fluorination of these side groups creates a dipole at the silicon atom, which leaves it more open to nucleophilic attack and results in a higher degree of hydrolysis.[27] This would lead to a larger number of nanoflakes and thicker shell walls compared to nonfluorinated silanes. The rate of polycondensation of the fluorinated silanes is still slower than that of pure TMOS due to steric hindrance and a smaller number of possible siloxane bonds that can be formed during polycondensation. The rate of hydrolysis of the methoxy/ethoxy groups from the silane is directly correlated to the rate of polycondensation between neighboring silanes. Therefore, the growth rate of the nanoflakes depends on the hydrolysis rate of the silanes. If diameter or thickness of the nanoflakes is decreased, and the nanoshells are composed of nanoflakes, it is more likely that thinner shell walls could be formed. It was found that the correlation coefficient between the nanoflake size and the shell thickness was 0.79 indicating a trend that smaller nanoflakes result in a decreased shell thickness.

There are at least three distinct regions in all of the nanoparticles. The inner dense layer is the black ring seen in images of all the particles (Layer A). The second layer is an intermediate less, dense layer between the black ring and the middle loose silica flakes (Layer B). The final layer is an irregular corona of attached exterior silica flakes (Layer C). A diagram of the different layers can be seen in Figure 6B, a larger diagram can be found in Figure S3 (Supporting Information). The **control** particles (Figure 6A,B) and the **phenyl-F** particles (Figure 6I,J) also appear to have a very thick Layer B. It is likely that the intermediate layer and the outer layer reduce the ultrasound performance of these particles. It should be noted that while the shell thickness appears to be the dominant property dictating the ultrasound activity of the nanoshells, it is not the only one. Other aspects that may play a role in the mechanical properties include the degree of condensation of the silica, the reactivity of the trialkoxysilanes, or the size of the nanoflakes that compose the particle shell.

The **C8** nanoshells and **phenyl** nanoshells have very similar ultrasound performance, but appear to have different nanostructures. Comparing the densest layer, whose fracture is postulated to occur at the minimum threshold, Layer A for the **phenyl** particles is 1.4 nm compared to 1.8 nm for the **C8** particles. Fracturing of the shell likely occurs during the rarefaction phase when the gas inside the nanoshell expands to uniformly apply pressure to the entire particle shell. By this metric, the **phenyl** formulation with the thinner Layer A should be significantly better than the **C8** formulation, but that is not observed. Layer B is on average 1.4 nm thinner in the **C8** formulation than the **phenyl** formulation which likely contributes to a greater number of points in which the Layer A is entirely exposed and able to easily fracture. It is hypothesized that the additional differences in **phenyl** and **C8** particles performance may be due to their differing nanoflake structures.

High-magnification TEM images were used to further analyze the nanoflakes dimensions. For the nanoflake thickness, it was assumed that the Layer A thicknesses correlates to the

Table 1. TEM-based shell analysis.

	Layer A [nm]	Layer B [nm]	Layer C [nm]	Shell thickness	Sum STD	Nanoflake diameter [nm]	Diameter STD [nm]	Min flake diameter [nm]	Max flake diameter [nm]
Control	3.8	18.3	26.9	49.0	13.7	10.8	4.7	4.4	22.8
C8	1.8	5.5	11.3	18.6	4.1	8.9	2.6	4.5	15.6
C8-F	2.4	5.0	19.3	26.6	3.8	8.8	3.1	4.8	16.6
Phenyl	1.4	6.9	10.2	18.5	4.5	6.5	2.0	2.4	11.9
Phenyl-F	2.9	17.8	13.6	34.4	5.8	8.5	2.5	4.3	14.4

Layer thicknesses were determined from pixel intensity versus distance plots (Figure S4, Supporting Information). Each plot was derived by averaging the pixel intensity of hundreds of line scans through an 80 nm arc of nanoshell wall across four different particles. For nanoflake measurements, 50 measurements were taken for each nanoparticle formulation in Image J from a minimum of four TEM images.

thickness of individual nanoflakes. Nanoflake diameters were quantified using the nanoflakes orthogonally aligned to the nanoshells to understand the effect on ultrasound performance of the nanoshells. A smaller flake diameter may increase ultrasound brightness by forming more nanoflake junctions that can fracture. All the R-substituted trialkoxysilane formulations have decreased nanoflake diameters compared to the control formulations, as shown in **Table 1**. The **C8**, **C8-F**, and **phenyl-F** particles all had nearly identical nanoflake diameters and diameter standard deviations. It is hypothesized that the smaller flake diameters observed in the **phenyl** particles, 6.5 nm, compared to 8.9 nm for **C8**, may contribute to the differences observed in ultrasound performance, despite the nearly indistinguishable shell thicknesses between the two formulations.

Brunauer-Emmett-Teller (BET) analysis was performed on the **control**, **phenyl**, and **phenyl-F** formulations (Table S2, Supporting Information). The pore diameters and surface area for all three formulations were similar. However, the pore volumes are increased for both the **phenyl-F** (0.15 $cm^3\ g^{-1}$) and **phenyl** (0.19 $cm^3\ g^{-1}$) formulations compared to the **control** (0.11 $cm^3\ g^{-1}$). The increased pore volume per gram for these formulations is consistent with the presence of smaller nanoflakes in these formulations. A smaller flake size at a constant mass would result in a larger number of grain boundaries, which is consistent with an increased pore volume per gram. Although the **phenyl** has the high pore volume per gram, it also has the thinnest shell; therefore, it has the lowest proportion of gas in the pores as compared to the interior of the particle.

Shown in **Table 2** are the correlation coefficients of nanoparticle properties (shell thickness and nanoflake diameter) with the particle performance measurements (MI threshold, imaging lifetime, imaging brightness at 1.5 MI, and HIFU pressure threshold). As can been seen in Table 2, there is a positive correlation between an increase in shell thickness/nanoflake diameter and increase in MI threshold and HIFU threshold, which means that a smaller shell thickness/nanoflake diameter is likely to reduce the thresholds and improve performance. There is a negative correlation between an increase in shell thickness/nanoflake diameter and an improvement in the continuous imaging longevity or CPS brightness of the nanoshells. This means that as the shell thickness/nanoflake diameter decreases, it is likely to improve imaging longevity and the brightness of the particles in CPS. Overall a decrease in shell thickness and nanoflake diameter correlated with improved ultrasound imaging performance. However, the correlation coefficient between shell thickness and ultrasound performance was always stronger than that the correlation coefficient between ultrasound performance and nanoflake diameter; in addition, the nanoflake size was strongly correlated with shell thickness (0.79). Therefore, the nanoflake diameter may not have an independent effect on ultrasound properties from shell thickness.

Table 2. Correlation of nanoshell parameters with ultrasound performance.

	Doppler MI threshold	HIFU threshold	Imaging lifetime	CPS brightness
Shell thickness	0.92	0.93	–0.85	–0.90
Nanoflake diameter	0.70	0.72	–0.66	–0.79

3. Conclusion

A method has been presented to prepare highly uniform 3D structures composed of nanoflakes with thicknesses ranging from 1.4 to 3.8 nm and diameters ranging from 2.4 to 22.8 nm. This allows the synthesis of iron–silica nanoshells of varying shell thicknesses with different mechanical strengths. It was found that by using trimethoxy(phenyl)silane for 70% of the silicon source and the remainder TMOS, 500 nm hollow ultrathin nanoshells that had a dense inner shell thickness of only 1.4 nm could be synthesized. Combining alkyl(trialkoxy)silane precursors with TMOS reduces the building block size of the average nanoflake diameter in the shell wall by as much as 40% to 6.5 nm. The ultrathin nanoshells synthesized with these modified silanes were mechanically weaker and exhibited improved performance as ultrasound contrast agents in vitro. Compared to **control** nanoshells synthesized with only TMOS, the newly developed particles have a tenfold increase in longevity during Doppler imaging. They also produce double the brightness during CPS imaging compared to **control** nanoshells, and became visible at a lower pressure threshold. The ultrasound data show that the ultrathin wall silica nanoshells have superior performance to commercial soft shell microbubbles for continuous imaging longevity in both Doppler and CPS imaging at clinically relevant powers. At an equivalent contained gas volume, the triethoxy(octyl)silane- and trimethoxy(phenyl) silane-substituted nanoshells generated greater contrast signal than commercial microbubbles at MI values exceeding 1.3 in

CPS imaging. To the authors' knowledge, this is the first report of a rigid particle generating more ultrasound contrast at equivalent gas volumes than soft microbubbles at clinically relevant power settings. In vivo rabbit experiments demonstrated that the ultrathin nanoshells remain stationary and produce color Doppler for as long as 11 d after intratumoral injection in highly vascularized VX2 tumors. These results show that nanoflake precursors can be used to synthesize 3D ultrathin structures and thereby alter critical mechanical properties of the nanoshells.

4. Experimental Section

Materials: Tetramethyl orthosilicate, triethoxy(octyl)silane, trimethoxy(phenyl)silane, 1H,1H,2H,2H-perfluorooctyltriethoxysilane, (pentafluorophenyl)triethoxysilane were all purchased from Sigma–Aldrich Corp (St. Louis, MO). 500 nm amino-polystyrene templates were purchased from Polysciences Inc. (Warrington, PA). Iron (III) ethoxide was acquired from Gelest Inc. (Moorisville, PA). PFP was acquired from Strem Chemicals (Newburyport, MA). Ultrasound images were acquired with a Seimens Sequoia 512 (Mountainview, CA) with an Acuson 15L8 imaging transducer. Sonic Concepts Inc. (Bothell, Washington) H-102 single element transducer was used to generate high-intensity ultrasound pulses that were powered by an AG 1006 Amplifier/Generator (Rochester, NY). Software used for analysis of data included Sante Dicom Viewer (Athens, Greece), Matlab (Natick, MA), and Microsoft Excel (Redmond, WA). Female rabbits were purchased from Western Oregon Rabbitry and individually housed in a UCSD vivarium facility. They were kept on a 12 h light/dark cycle and given water and Harlan Teklad commercial pellet diet ad libitum. All animal procedures were approved by the UCSD IACUC. Tumors were implanted when rabbits were between 2.5 and 3.0 kg.

Synthesis: Control nanoshells were synthesized as previously described.[23] In brief, 50 µL of amino-polystyrene templates were added to 1 mL of anhydrous ethanol. Iron (III) ethoxide was suspended in a second aliquot of anhydrous ethanol at 20 mg mL^{-1}. 10 µL of this solution was mixed with 2.7 µL of TMOS, and the entirety was added to the template solution. The mixture was mixed for 5 h, centrifuged and washed twice with ethanol, and left to dry in air overnight. The dried particles were calcined for 18 h at 550 °C. The yield per Eppendorf tube of final product ranged from 400 to 800 µg and typically the products from 24 eppendorf tubes were added to a crucible for calcination. The synthesis of other formulations was similar to that of the control nanoshells. The molar quantity of silicon precursor was kept constant; however, only 30% of it was derived from TMOS and the remaining 70% was derived from one of the following R-group-substituted trialkoxysilanes: triethoxy(octyl)silane "**C8**," trimethoxyphenylsilane "**Phenyl**," 1H,1H,2H,2H-perfluorooctyltriethoxysilane "**C8-F**," and (pentafluorophenyl)triethoxysilane "**Phenyl-F**." Other ratio formulations were synthesized, but the 70:30 molar ratio was the highest ratio at which all formulations produced uniform particles with no fractured shells or colloidal silica. As a result, the 70:30 molar ratio was used for all in vitro experiments reported in this paper. Structures of the R-group-substituted trialkoxysilanes additives can be seen in Figure 1A. For the new formulations, R-group-substituted trialkoxysilanes were mixed with TMOS and iron ethoxide before addition to the template solution. After calcination, the particles were stored dried and, subsequently, filled with perfluorocarbon gas as previously described.[13,22] In brief, dry particles were placed in an amber vial with a self-sealing silicone top and then evacuated on a Schlenk line. Afterward, PFP liquid was vaporized in a gas syringe and injected into the amber vial. This process was repeated three times to ensure that atmospheric gas was removed and replaced with PFP. Subsequently, water was added to the amber vial, which sealed the very insoluble fluorous phase within the nanoshells.

Ultrasound Experiments: Prior to ultrasound testing each formulation, at least 24 batches of nanoshells were homogenized in a single tube to reduce batch-to-batch variation within a single formulation. All ultrasound tests were repeated at minimum in triplicate and on multiple days, with nanoshells filled with gas the day of each experiment. For all ultrasound experiments, gas-filled nanoshells were suspended in a pipette bulb at a concentration of 400 µg mL^{-1}. The pipette bulb was clamped perpendicular to the ultrasound imaging transducer, typically on the top of the HIFU focusing cone in a water bath, as shown in Figure 1B. Two different types of experiments were performed; the first used the imaging transducer alone. To quantify the sensitivity of the particles to ultrasound, samples were exposed to continuous color Doppler imaging at 1.9 MI for 180 min, or until the color signal could no longer be observed, whichever was shorter. To assess image brightness generation, samples were imaged with CPS at 7 MHz, which was shown to generate the strongest signal from nanoshells.[22] Images were acquired continuously as the MI was increased from 0.06 to the maximum clinically allowable MI of 1.9 to define the minimum threshold for signal generation and to quantify the image brightness produced. Each measurement on Definity microbubbles at each MI was done using a pristine sample, which had no prior exposure to ultrasound. Peak brightnesses in the CPS images acquired at each MI were recorded. The second experiment utilized the HIFU transducer for signal generation. This delivered 20 µs bursts at 1.1 MHz, whose pressure amplitude was slowly increased until a contrast signal was detected on CPS images. To monitor the particles during the HIFU pulse, an imaging transducer was aligned orthogonally and confocally as to not interfere with the HIFU transducer. The imaging transducer was operated in CPS mode at 0.1 MI, which was well below the pressures produced by the HIFU transducer. This technique is denoted as single-pulse stimulated imaging.

Tumor Implantation and Intratumoral Imaging Study: Animals were anesthetized with an SQ injection of ketamine/xylazine cocktail and placed onto a heating pad at 37 °C. The area surrounding the thighs of the hind legs was shaved and depilated and the skin was disinfected with a chlorhexidine solution. A 1–2 cm vertical incision was cut in the skin in the thigh to expose the muscle, and blunt dissection was employed to separate the muscle fibers. A trimmed and cleaned VX2 lung metastasis harvested from a carrier rabbit was inserted into the muscle pocket, which was then closed with a single stitch of absorbable suture. The skin was then closed with nylon suture and skin glue. The animal was allowed to recover with analgesics. The animals were fitted with Elizabethan collars, and returned to their cages upon sternal recumbence. Incision sites were checked daily for 10 d, with analgesics and antibiotics administered as necessary. Sutures and collars were removed once the wound had healed. Checks continued twice weekly until animals were studied. All imaging studies occurred on rabbits anesthetized with isoflurane gas and oxygen. 100 µL of nanoshells at 4 mg mL^{-1} was injected intratumorally into VX2 tumor-bearing rabbits and imaged over the course of 13 d. The ultrathin nanoshells used in this experiment were derived from a 55:45 molar ratio of trimethoxy(phenyl) silane:TMOS ratio due to improved synthetic yield and nearly identical ultrasound characteristics.

Electron Microscopy: For all electron microscopy measurements, the particles were suspended in ethanol and sonicated in a bath sonicator for 30 min and subsequently drop cast onto a carbon tape substrate for SEM analysis or onto a lacey carbon film grid substrate for TEM characterization. TEM imaging was performed in a JEOL (JEOL, Tokyo, Japan) ARM200F operated at 200 kV. Values in Table 1 were attained by analyzing images acquired by TEM in Image J. For analysis of the different layers within the nanoshells, areas of interest were first demarcated along the shell walls. Line traces for pixel intensity were performed through the shell walls radially and were averaged along the shell walls orthogonally through the line scans. This produced a curve of average pixel intensity versus distance (Figure S4, Supporting Information), which contained three unique regions defined by varying inflection points and slope. These unique regions were defined as Layers A–C based on average pixel intensity. Since TEM images are 2D projections, the nanoflake values in Table 1 were acquired by measuring

only the single largest parameter for each nanoflake that was clearly distinguishable with high-resolution TEM at 150K magnification.

Supporting Information

Supporting Information is available from the Wiley Online Library or from the author.

Acknowledgements

A.L. and J.W. contributed equally to this work. This research was supported by the Samsung Advanced Institute of Technology, Grant No. 20125011 and NIH IMAT 1R33CA177449-01A1. This research was supported in part by the Louis A. Beecherl, Jr. endowment funds. Individual student funding was provided by NIH Ruth L. Kirschstein National Research Service Award F31 Fellowship (NIH Grant No. 1F31CA174276), and the NIH—Cross Training Translation Cancer Researchers in Nanotechnology (CRIN) grant (NIH 3 R25 CA 153915). These experiments utilized equipment provided by the In Vivo Cancer and Molecular Imaging Center (ICMIC) P50-CA128346.

Received: February 12, 2015
Revised: April 24, 2015
Published online: May 21, 2015

[1] a) F. Chen, H. Hong, Y. Zhang, H. F. Valdovinos, S. Shi, G. S. Kwon, C. P. Theuer, T. E. Barnhart, W. Cai, *ACS Nano* **2013**, *7*, 9027 b) W. Fang, J. Yang, J. Gong, N. Zheng, *Adv. Funct. Mater.* **2012**, *22*, 842; c) S. Giri, B. G. Trewyn, M. P. Stellmaker, V. S. Y. Lin, *Angew. Chem. Int. Ed.* **2005**, *44*, 5038; d) H. J. Kim, H. Matsuda, H. Zhou, I. Honma, *Adv. Mater.* **2006**, *18*, 3083; e) S. D. Kong, W. Zhang, J. H. Lee, K. Brammer, R. Lal, M. Karin, S. Jin, *Nano Lett.* **2010**, *10*, 5088.

[2] N. Ž. Knežević, B. G. Trewyn, V. S. Y. Lin, *Chem. Eur. J.* **2011**, *17*, 3338.

[3] a) I. Ortac, D. Simberg, Y.-S. Yeh, J. Yang, B. Messmer, W. C. Trogler, R. Y. Tsien, S. C. Esener, *Nano Lett.* **2014**; b) I. I. Slowing, B. G. Trewyn, V. S. Y. Lin, *J. Am. Chem. Soc.* **2007**, *129*, 8845; c) J. F. Díaz, K. J. Balkus Jr., *J. Mol. Catal. B* **1996**, *2*, 115.

[4] a) K. M. L. Taylor, J. S. Kim, W. J. Rieter, H. An, W. Lin, W. Lin, *J. Am. Chem. Soc.* **2008**, *130*, 2154; b) J. L. Vivero-Escoto, K. M. L. Taylor-Pashow, R. C. Huxford, J. Della Rocca, C. Okoruwa, H. An, W. Lin, W. Lin, *Small* **2011**, *7*, 3519; c) H. Hu, H. Zhou, J. Du, Z. Wang, L. An, H. Yang, F. Li, H. Wu, S. Yang, *J. Mater. Chem.* **2011**, *21*, 6576; d) S. Santra, R. P. Bagwe, D. Dutta, J. T. Stanley, G. A. Walter, W. Tan, B. M. Moudgil, R. A. Mericle, *Adv. Mater.* **2005**, *17*, 2165.

[5] a) K. Nozawa, H. Gailhanou, L. Raison, P. Panizza, H. Ushiki, E. Sellier, J. P. Delville, M. H. Delville, *Langmuir* **2004**, *21*, 1516; b) Q. Cai, W.-Y. Lin, F.-S. Xiao, W.-Q. Pang, X.-H. Chen, B.-S. Zou, *Microporous Mesoporous Mater.* **1999**, *32*, 1; c) J. Yang, J. U. Lind, W. C. Trogler, *Chem. Mater.* **2008**, *20*, 2875.

[6] F. Caruso, R. A. Caruso, H. Möhwald, *Science* **1998**, *282*, 1111.

[7] T. Liu, L. Li, X. Teng, X. Huang, H. Liu, D. Chen, J. Ren, J. He, F. Tang, *Biomaterials* **2011**, *32*, 1657.

[8] G. Xie, J. Sun, G. Zhong, L. Shi, D. Zhang, *Arch. Toxicol.* **2010**, *84*, 183.

[9] a) Y. Zhao, B. G. Trewyn, I. I. Slowing, V. S. Y. Lin, *J. Am. Chem. Soc.* **2009**, *131*, 8398; b) D. Zhao, J. Feng, Q. Huo, N. Melosh, G. H. Fredrickson, B. F. Chmelka, G. D. Stucky, *Science* **1998**, *279*, 548.

[10] C.-P. Tsai, C.-Y. Chen, Y. Hung, F.-H. Chang, C.-Y. Mou, *J. Mater. Chem.* **2009**, *19*, 5737.

[11] a) T. Yokoi, H. Yoshitake, T. Tatsumi, *J. Mater. Chem.* **2004**, *14*, 951; b) M. C. Burleigh, M. A. Markowitz, M. S. Spector, B. P. Gaber, *J. Phys. Chem. B* **2001**, *105*, 9935; c) S. Huh, J. W. Wiench, J.-C. Yoo, M. Pruski, V. S. Y. Lin, *Chem. Mater.* **2003**, *15*, 4247; d) X. Wang, H. Chen, Y. Chen, M. Ma, K. Zhang, F. Li, Y. Zheng, D. Zeng, Q. Wang, J. Shi, *Adv. Mater.* **2012**, *24*, 785.

[12] K. K. Pohaku Mitchell, A. Liberman, A. C. Kummel, W. C. Trogler, *J. Am. Chem. Soc.* **2012**, *134*, 13997.

[13] H. P. Martinez, Y. Kono, S. L. Blair, S. Sandoval, J. Wang-Rodriguez, R. F. Mattrey, A. C. Kummel, W. C. Trogler, *MedChemComm* **2010**, *1*, 266.

[14] L. Zhang, M. D'Acunzi, M. Kappl, G. n. K. Auernhammer, D. Vollmer, C. M. van Kats, A. van Blaaderen, *Langmuir* **2009**, *25*, 2711.

[15] A. Liberman, N. Mendez, W. C. Trogler, A. C. Kummel, *Surf. Sci. Rep.* **2014**, *69*, 132.

[16] M. Mazur, *Electrochem. Commun.* **2004**, *6*, 400.

[17] a) S. Li, B. Long, Z. Wang, Y. Tian, Y. Zheng, Q. Zhang, *J. Solid State Chem.* **2010**, *183*, 957; b) M. Reddy, T. Yu, C.-H. Sow, Z. X. Shen, C. T. Lim, G. Subba Rao, B. Chowdari, *Adv. Funct. Mater.* **2007**, *17*, 2792; c) E. Hosono, S. Fujihara, I. Honma, M. Ichihara, H. Zhou, *J. Power Sources* **2006**, *158*, 779.

[18] R. Cui, W. Lu, L. Zhang, B. Yue, S. Shen, *J. Phys. Chem. C* **2009**, *113*, 21520.

[19] J.-U. Voigt, *Methods* **2009**, *48*, 92.

[20] C. Sonne, F. Xie, J. Lof, J. Oberdorfer, P. Phillips, E. Carr Everbach, T. R. Porter, *J. Am. Soc. Echocardiogr.* **2003**, *16*, 1178.

[21] a) C. N. Ta, A. Liberman, H. Paul Martinez, C. V. Barback, R. F. Mattrey, S. L. Blair, W. C. Trogler, A. C. Kummel, Z. Wu, *J. Vac. Sci. Technol. B* **2012**, *30*, 02C104; b) D. Cosgrove, *Eur. J. Radiol.* **2006**, *60*, 324.

[22] A. Liberman, H. P. Martinez, C. N. Ta, C. V. Barback, R. F. Mattrey, Y. Kono, S. L. Blair, W. C. Trogler, A. C. Kummel, Z. Wu, *Biomaterials* **2012**, *33*, 5124.

[23] A. Liberman, Z. Wu, C. V. Barback, R. Viveros, S. L. Blair, L. G. Ellies, D. R. Vera, R. F. Mattrey, A. C. Kummel, W. C. Trogler, *ACS Nano* **2013**, *7*, 6367.

[24] N. G. Rognin, P. Frinking, M. Costa, M. Arditi, presented at *IEEE Ultrason. Symp., IUS 2008* Beijing, November **2008.**

[25] M. G. Voronkov, V. P. Mileshkevich, Y. A. Yuzhelevskii, *The Siloxane Bond*, Consultants Bureau, New York **1978**, p 170.

[26] M.-C. Brochier Salon, P.-A. Bayle, M. Abdelmouleh, S. Boufi, M. N. Belgacem, *Colloids Surf., A* **2008**, *312*, 83.

[27] C. J. Brinker, G. W. Scherer, *Sol-Gel Science: The Physics and Chemistry of Sol-Gel Processing*, Academic Press, San Diego **2013**.